Energetic mid-IR femtosecond pulse generation by self-defocusing soliton-induced dispersive waves in a bulk quadratic nonlinear crystal

Zhou, Binbin; Guo, Hairun; Bache, Morten

Published in:
Optics Express

Link to article, DOI:
10.1364/OE.23.006924

Publication date:
2015

Document Version
Publisher's PDF, also known as Version of record

Energetic mid-IR femtosecond pulse generation by self-defocusing soliton-induced dispersive waves in a bulk quadratic nonlinear crystal

Binbin Zhou, Hairun Guo, and Morten Bache*

DTU Fotonik, Department of Photonics Engineering, Technical University of Denmark, DK-2800 Kgs. Lyngby, Denmark

**moba@fotonik.dtu.dk*

Abstract: Generating energetic femtosecond mid-IR pulses is crucial for ultrafast spectroscopy, and currently relies on parametric processes that, while efficient, are also complex. Here we experimentally show a simple alternative that uses a single pump wavelength without any pump synchronization and without critical phase-matching requirements. Pumping a bulk quadratic nonlinear crystal (unpoled $LiNbO_3$ cut for noncritical phase-mismatched interaction) with sub-mJ near-IR 50-fs pulses, tunable and broadband ($\sim 1,000$ cm^{-1}) mid-IR pulses around 3.0 μm are generated with excellent spatio-temporal pulse quality, having up to 10.5 μJ energy (6.3% conversion). The mid-IR pulses are dispersive waves phase-matched to near-IR self-defocusing solitons created by the induced self-defocusing cascaded nonlinearity. This process is filament-free and the input pulse energy can therefore be scaled arbitrarily by using large-aperture crystals. The technique can readily be implemented with other crystals and laser wavelengths, and can therefore potentially replace current ultrafast frequency-conversion processes to the mid-IR.

OCIS codes: (320.7110) Ultrafast nonlinear optics; (190.5530) Pulse propagation and temporal solitons; (320.6629) Supercontinuum generation; (320.2250) Femtosecond phenomena.

References and links

1. M. L. Cowan, B. D. Bruner, N. Huse, J. R. Dwyer, B. Chugh, E. T. J. Nibbering, T. Elsaesser, and R. J. D. Miller, "Ultrafast memory loss and energy redistribution in the hydrogen bond network of liquid H_2O," Nature **434,** 199–202 (2005).
2. K. Ramasesha, L. D. Marco, A. Mandan, and A. Tokmakoff, "Water vibrations have strongly mixed intra- and intermolecular character," Nat. Chem. **5,** 935–640 (2013).
3. F. Seifert, V. Petrov, and M. Woerner, "Solid-state laser system for the generation of midinfrared femtosecond pulses tunable from 3.3 to 10 μm," Opt. Lett. **19,** 2009–2011 (1994).
4. R. A. Kaindl, M. Wurm, K. Reimann, P. Hamm, A. M. Weiner, and M. Woerner, "Generation, shaping, and characterization of intense femtosecond pulses tunable from 3 to 20 μm," J. Opt. Soc. Am. B **17,** 2086–2094 (2000).
5. H. Nienhuys, P. C. M. Planken, R. A. Van Santen, and H. J. Bakker, "Generation of mid-infrared pulses by $\chi^{(3)}$ difference frequency generation in CaF_2 and BaF_2," Opt. Lett. **26,** 1350–1352 (2001).
6. T. Fuji, and T. Suzuki, "Generation of sub-two-cycle mid-infrared pulses by four-wave mixing through filamentation in air," Opt. Lett. **32,** 3330–3332 (2007).
7. P. B. Petersen, and A. Tokmakoff, "Source for ultrafast continuum infrared and terahertz radiation," Opt. Lett. **35,** 1962–1964 (2010).

#223288 - $15.00 USD Received 14 Jan 2015; revised 3 Mar 2015; accepted 3 Mar 2015; published 6 Mar 2015

8. D. V. Skryabin, F. Luan, J. C. Knight, and P. St. J. Russell, "Soliton self-frequency shift cancellation in photonic crystal fibers," Science **301,** 1705–1708 (2003).
9. J. M. Dudley, G. Genty, and S. Coen, "Supercontinuum generation in photonic crystal fiber," Rev. Mod. Phys. **78,** 1135–1184 (2006).
10. D. V. Skryabin and A. V. Gorbach, "Colloquium: Looking at a soliton through the prism of optical supercontinuum," Rev. Mod. Phys. **82,** 1287–1299 (2010).
11. L. Tartara, I. Cristiani, and V. Degiorgio, "Dispersive wave generation by solitons in microstructured optical fibers," Appl. Phys. B **77,** 307–311 (2003).
12. G. Chang, L. J. Chen, and F. X. Kärtner, "Highly efficient Cherenkov radiation in photonic crystal fibers for broadband visible wavelength generation," Opt. Lett. **35,** 2361–2363 (2010).
13. K. F. Mak, J. C. Travers, P. Hölzer, N. Y. Joly, and P. St. J. Russell, "Tunable vacuum-UV to visible ultrafast pulse source based on gas-filled Kagome-PCF," Opt. Express **21,** 10942–10953 (2013).
14. P. Falk, M. H. Frosz, O. Bang, L. Thrane, P. E. Andersen, A. O. Bjarklev, K. P. Hansen, and J. Broeng, "Broadband light generation at 1300 nm through spectrally recoiled solitons and dispersive waves," Opt. Lett. **33,** 621–623 (2008).
15. M. Kolesik, L. Tartara, and J. V. Moloney, "Effective three-wave-mixing picture and first Born approximation for femtosecond supercontinua from microstructured fibers," Phys. Rev. A **82,** 045802 (2010).
16. J. H. Yuan, X. Z. Sang, Q. Wu, C. X. Yu, K. R. Wang, B. B. Yan, X. W. Shen, Y. Han, G. Y. Zhou, Y. Semenova, G. Farrell, and L. T. Hou, "Widely tunable broadband deep-ultraviolet to visible wavelength generation by the cross phase modulation in a hollow-core photonic crystal fiber cladding," Laser Phys. Lett. **10,** 045405 (2013).
17. I. Golub, "Optical characteristics of supercontinuum generation," Opt. Lett. **15,** 305–307 (1990).
18. E. T. J. Nibbering, P. F. Curley, G. Grillon, B. S. Prade, M. A. Franco, F. Salin, and A. Mysyrowicz, "Conical emission from self-guided femtosecond pulses in air," Opt. Lett. **21,** 62–64 (1996).
19. M. Kolesik, E. M. Wright, and J. V. Moloney, "Interpretation of the spectrally resolved far field of femtosecond pulses propagating in bulk nonlinear dispersive media," Opt. Express **13,** 10729–10741 (2005).
20. D. Faccio, A. Averchi, A. Couairon, M. Kolesik, J. V. Moloney, A. Dubietis, G. Tamosauskas, P. Polesana, A. Piskarskas, and P. Di Trapani, "Spatio-temporal reshaping and X Wave dynamics in optical filaments," Opt. Express **15,** 13077–13095 (2007).
21. E. Rubino, J. McLenahan, S. C. Kehr, F. Belgiorno, D. Townsend, S. Rohr, C. E. Kuklewicz, U. Lenohardt, F. König, and D. Faccio, "Negative-frequency resonant radiation," Phys. Rev. Lett. **108,** 253901 (2012).
22. M. Bache, O. Bang, W. Krolikowski, J. Moses and F. W. Wise, "Limits to compression with cascaded quadratic soliton compressors," Opt. Express **16,** 3273–3287 (2008).
23. M. Bache, O. Bang, B. B. Zhou, J. Moses, and F. W. Wise, "Optical Cherenkov radiation in ultra-fast cascaded second-harmonic generation," Phys. Rev. A **82,** 063806 (2010).
24. M. Bache, O. Bang, B. B. Zhou, J. Moses, and F. W. Wise, "Optical Cherenkov radiation by cascaded nonlinear interaction: an efficient source of energetic few-cycle near- to mid-IR pulses," Opt. Express **19,** 22557–22562 (2011).
25. R. DeSalvo, D. Hagan, M. Sheik-Bahae, G. Stegeman, E. W. Van Stryland, and H. Vanherzeele, "Self-focusing and self-defocusing by cascaded second-order effects in KTP," Opt. Lett. **17,** 28–30 (1992).
26. B. B. Zhou, A. Chong, F. W. Wise and M. Bache, "Ultrafast and octave-spanning optical nonlinearities from strongly phase-mismatched cascaded interaction," Phys. Rev. Lett. **109,** 043902 (2012).
27. S. Ashihara, T. Shimura, K. Kuroda, N. E. Yu, S. Kurimura, K. Kitamura, M. Cha, and T. Taira, "Optical pulse compression using cascaded quadratic nonlinearities in periodically poled lithium niobate," Appl. Phys. Lett. **84,** 1055–1057 (2004).
28. X. Zeng, S. Ashihara, X. Chen, T. Shimura and K. Kuroda, "Two-color pulse compression in aperiodically-poled lithium niobate," Opt. Commun. **281,** 4499–4503 (2008).
29. S. Ashihara, J. Nishina, T. Shimura and K. Kuroda, "Soliton compression of femtosecond pulses in quadratic media," J. Opt. Soc. Am. B **19,** 2505–2510 (2002).
30. J. Moses, and F. W. Wise, "Soliton compression in quadratic media: high-energy few-cycle pulses with a frequency-doubling crystal," Opt. Lett. **31,** 1881–1883 (2006)
31. B. B. Zhou, H. R. Guo and M. Bache, "Soliton-induced nonlocal resonances observed through high-intensity tunable spectrally compressed second-harmonic peaks," Phys. Rev. A **90,** 013823 (2014).
32. C. Langrock, M. M. Fejer, I. Hartl and M. E. Fermann, "Generation of octave-spanning spectra inside reverse-proton-exchanged periodically poled lithium niobate waveguides," Opt. Lett. **32,** 2478–2480 (2007).
33. C. R. Phillips, C. Langrock, J. S. Pelc, M. M. Fejer, J. Jiang, M. E. Fermann and I. Hartl, "Supercontinuum generation in quasi-phase-matched $LiNbO_3$ waveguide pumped by a Tm-doped fiber laser system," Opt. Lett. **36,** 3912–3914 (2011).
34. H. R. Guo, B. B. Zhou, M. Steinert, F. Setzpfandt, T. Pertsch, H. P. Chung, Y. H. Chen and M. Bache, "Supercontinuum generation in quadratic nonlinear waveguides without quasi-phase matching," Opt. Lett. **40,** 629–632 (2015).
35. C. R. Phillips, C. Langrock, J. S. Pelc, M. M. Fejer, I. Hartl, and M. E. Fermann, "Supercontinuum generation in quasi-phasematched waveguides," Opt. Express **19**, 18754–18773 (2011).

#223288 - $15.00 USD Received 14 Jan 2015; revised 3 Mar 2015; accepted 3 Mar 2015; published 6 Mar 2015

36. M. Bache, O. Bang, J. Moses and F. W. Wise, "Nonlocal explanation of stationary and nonstationary regimes in cascaded soliton pulse compression," Opt. Lett. **32,** 2490–2492 (2007).
37. N. Akhmediev and M. Karlsson, "Cherenkov radiation emitted by solitons in optical fibers," Phys. Rev. A **51,** 2602–2607 (1995).
38. M. Bache, J. Moses, and F. W. Wise, "Scaling laws for soliton pulse compression by cascaded quadratic nonlinearities," J. Opt. Soc. Am. B **24,** 2752–2762 (2007).
39. M. Bache and R. Schiek, "Review of measurements of Kerr nonlinearities in lithium niobate: the role of the delayed Raman response," arXiv:1211.1721v1 (2012).
40. H. Guo, X. Zeng, B. Zhou and M. Bache, "Nonlinear wave equation in frequency domain: accurate modeling of ultrafast interaction in anisotropic nonlinear media," J. Opt. Soc. Am. B **30,** 494–504 (2013).
41. M. Bache, H. R. Guo and B. B. Zhou, "Generating mid-IR octave-spanning supercontinua and few-cycle pulses with solitons in phase-mismatched quadratic nonlinear crystals," Opt. Mater. Express **3,** 1647–1657 (2013).
42. B. Zhou, H. Guo, X. Liu, and M. Bache, ""Octave-spanning mid-IR supercontinuum generation with ultrafast cascaded nonlinearities," in Proceedings of CLEO: 2014, OSA Technical Digest (online) (Optical Society of America, 2014), paper JTu4A.24.

1. Introduction

Intense ultrashort mid-IR (MIR) pulses with microjoule pulse energy are highly important for the study of molecular vibrations [1, 2], in particular in the 2,800-4,000 cm^{-1} region ($\lambda = 2.5 - 3.6\ \mu$m) as it contains the stretching modes of C-H, N-H and O-H bonds. The commonly used methods for generating high-energy ultrashort MIR pulses are based on nonlinear optical parametric processes. One of the most popular methods is optical parametric amplification (OPA) [3], and an extra difference-frequency generation (DFG) stage is often integrated to further extend the output wavelength range [4]. These wavelength down-conversion techniques enable the generation of tunable MIR pulses in a broad spectral range and have good conversion efficiencies. The downside is that the processes require critical phase-matching condition and synchronized pump wavelengths, which complicates the setup for MIR generation. Four-wave mixing in $\chi^{(3)}$ media has also been reported for intense MIR pulse generation [5–7], which also involve synchronized pump wavelengths, and typically bear rather low conversion efficiencies.

Here we conduct an experiment employing a simpler technique: a bulk quadratic nonlinear crystal is pumped with a single near-IR (NIR) femtosecond pulse, and if the pump pulse is intense enough to excite a NIR soliton, it is possible to efficiently transfer some of the soliton energy into an energetic MIR femtosecond pulse. This MIR pulse is generated as a so-called dispersive wave (DW), and the wavelength of the generated MIR radiation is determined by a phase-matching condition between the soliton and the DW. The scheme relies on the excitation of a self-defocusing soliton, which here is done in a standard bulk quadratic $\chi^{(2)}$ nonlinear crystal, cut for strongly phase mismatched second-harmonic generation (SHG) and pumped in the normal group-velocity dispersion (GVD) regime. Due to the self-defocusing nature of the soliton the DW will automatically be emitted in the long-wavelength side of the soliton in the anomalous GVD regime, which for the crystal we use (lithium niobate, LN) is in the MIR.

Soliton-induced DWs (also denoted "resonant radiation" or "Cherenkov radiation") have been intensively investigated for generating waves at new frequencies, e.g. in fiber supercontinuum generation [8–10]. They were also used for wavelength conversion, especially in the short-wavelength side of the soliton (normal dispersion regime) [11–13]. Inside specially designed photonic crystal fibers with small cores and double zero-dispersion wavelengths, fiber-based DWs located to the red side of the soliton were also reported [14–16], and with a NIR pump, the longest obtained emission wavelength is about 2.2 μm [16]. One of the major limitations of fiber-based DW generation is the limited pulse energy, especially for DW generation on the red side, which requires fibers with double zero-dispersion wavelengths. Using bulk materials obviously allows to use a much higher pulse energy, but much less effort has been made for this research direction. In bulk, the self-focusing Kerr nonlinearity tends to generate filamentation,

#223288 - $15.00 USD Received 14 Jan 2015; revised 3 Mar 2015; accepted 3 Mar 2015; published 6 Mar 2015

and bulk DWs have mainly been observed in connection with conical emission or the characteristic spatio-temporal spectra of the self-focusing filamentation [17–20]. Another issue is that in bulk self-focusing Kerr media the DW is always located on the blue side of the soliton, such as the UV DWs recently observed [21], and can therefore not be used for downconversion to the MIR.

Using instead a self-defocusing nonlinearity, the soliton formation will be filament free and the DW will be located on the red side of the soliton [22, 23]. Such a self-defocusing effect can be generated by phase-mismatched (cascaded) quadratic nonlinearities, e.g. SHG [25]. Under strong phase mismatch, the pump experiences a Kerr-like nonlinearity characterized by the cascaded nonlinear refractive index $n^I_{2,\mathrm{casc}} \propto -d^2_{\mathrm{eff}}/\Delta k$, which is negative when the phase-mismatch parameter is positive, $\Delta k = k_2 - 2k_1 > 0$. Here d_{eff} is the effective quadratic nonlinearity and k_1 and k_2 are the wavenumbers of the pump and second harmonic (SH), respectively.

We will here investigate an LN crystal, which is attractive because its anomalous dispersion regime lies in the MIR, and this is therefore also the regime where DW emission is predicted [24]. In order to observe such a DW, a NIR self-defocusing soliton must first be excited. The first experimental realization of soliton self-compression and supercontinuum generation in a bulk LN crystal cut for noncritical interaction was demonstrated by some of us [26]. Self-defocusing solitons have also been observed experimentally using bulk crystals cut for critical SHG, namely in periodically poled LN [27, 28], and in beta-barium borate (β-BaB_2O_4) [23, 29–31]. However, none of these experiments could observe a DW and the closest cases were [23], where a linear NIR wave and a soliton were identified and by calculating the four-wave mixing interaction (a non-degenerate version of the DW phase-matching condition) a DW around 2.0 μm was predicted, and [26] where the NIR soliton was predicted to give DW radiation beyond 3.0 μm. In both of these cases the long-wavelength contents of the spectra could not be measured to confirm this. Supercontinuum generation has also been observed from cascaded SHG in LN waveguides, both in periodically-poled [32, 33] and unpoled waveguides [34]. Although a mid-IR peak around 2.8 μm was found in [32], it was later explained by cascaded difference-frequency generation of the soliton and the SH [35], and [34] could not observe DWs as the waveguides did not provide sufficient guiding in the long-wavelength regime.

The goals of the proof-of-principle experiment we here conduct are (a) to show that with a single input pulse it is possible to get μJ-level MIR femtosecond radiation through DW formation in a short piece of nonlinear crystal and (b) to clearly observe and characterize the MIR DW from a self-defocusing cascaded quadratic nonlinearity for the first time. Due to the simple pumping scheme and filament-free nature of the interaction this setup is very scalable in energy. The MIR peak wavelength is tunable by changing the pump wavelength, and the protocol can be generalized to other nonlinear crystals and pumping wavelengths.

2. Experimental setup

The experimental setup for generating the MIR DW is identical to the one reported in [26]. It is rather simple, consisting of a NIR pump laser source (here a 1 kHz commercial OPA system), which is loosely collimated and projected to the quadratic nonlinear crystal through the telescope consisting of two curved silver reflectors. The beam spot size on the crystal was 0.6 mm full-width-at-half-max (FWHM), which is large enough to avoid beam divergence in the short crystal, and the large spot size is also intended to keep diffraction effects to a minimum. The pulse durations of the NIR pumps were around 50 fs and nearly transform limited. A neutral density filter wheel was used in front of the telescope to adjust the pump intensity. For spectral characterization, an InGaAs CCD-based spectrometer is used for the wavelength below 2300 nm. A grating monochromator and HgCdTe (MCT) detector connected with a box-car

#223288 - $15.00 USD Received 14 Jan 2015; revised 3 Mar 2015; accepted 3 Mar 2015; published 6 Mar 2015

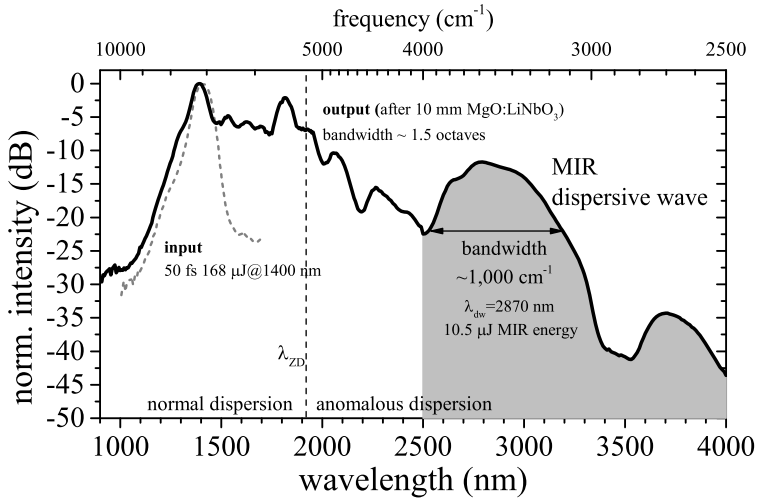

Fig. 1. Normalized input and output spectra from a 10 mm bulk LN crystal pumped with 50 fs 168 μJ pulses centered at 1.4 μm and having 0.8 TW/cm^2 peak intensity. A filament-free octave-spanning supercontinuum is formed, including an energetic, broadband DW in the MIR around 2.87 μm.

integrator was used to record the MIR spectrum.

Just as in [26] we used a 10-mm-long, 5% MgO-doped congruent LN ($LiNbO_3$, 10×10 mm^2 aperture, Altechna). The pump (frequency ω_1) and the SH (frequency $\omega_2 = 2\omega_1$) are both *e*-polarized beams with polarization along the vertical optical *Z* axis. The crystal was Y-cut ($\theta = \pi/2$, $|\phi| = \pi/2$) for noncritical (type 0) $ee \to e$ SHG; note that in [26] we mistakenly reported the crystal to be X-cut. This cut has $\Delta k \simeq +500$ mm^{-1}, resulting in a defocusing cascaded nonlinearity. Traditionally in type 0 cascading, periodic poling would be employed to reduce Δk and thereby increase the cascading strength, but we choose not to do this as it would leave the cascaded nonlinearity resonant and narrow-band [22,26,36]. Despite the large Δk, the cascaded nonlinearity is still strong because of the large $d_{\rm eff} = d_{33} = 25$ pm/V. What matters is that the self-defocusing cascading nonlinearity is larger than the material self-focusing electronic Kerr nonlinearity so the pump effectively experiences a self-defocusing Kerr effect. An advantage of such a large Δk is actually that the SH conversion remains insignificant, typically on the order of a few percent. Note that the noncritical interaction has zero spatial walk-off (as opposed to the critical SHG scheme in [23, 27–31]).

3. Experimental results and comparison with numerical simulations

3.1. Supercontinuum generation and MIR DW formation

With this setup significant spectral broadening occurred when gradually increasing the pump intensity, and Fig. 1 shows a supercontinuum under 1.4 μm and 0.8 TW/cm^2 pump condition. Similar spectra were observed at other pump wavelengths in the range $\lambda_1 = 1.2 - 1.45$ μm. Such an amount of spectral broadening is enabled by the ultra-broadband nature of the non-critical strongly phase-mismatched SHG process, which gives rise to soliton self-compression to few-cycle duration; indeed LN is predicted to support self-defocusing solitons in the pump regime we investigate [26]. After the soliton self-compression point a supercontinuum will form such as the one in Fig. 1, and it shows tremendous spectral extensions in the red side of the pump and goes far beyond the zero-dispersion wavelength $\lambda_{\rm ZD} = 1.92$ μm. As we will

#223288 - $15.00 USD Received 14 Jan 2015; revised 3 Mar 2015; accepted 3 Mar 2015; published 6 Mar 2015

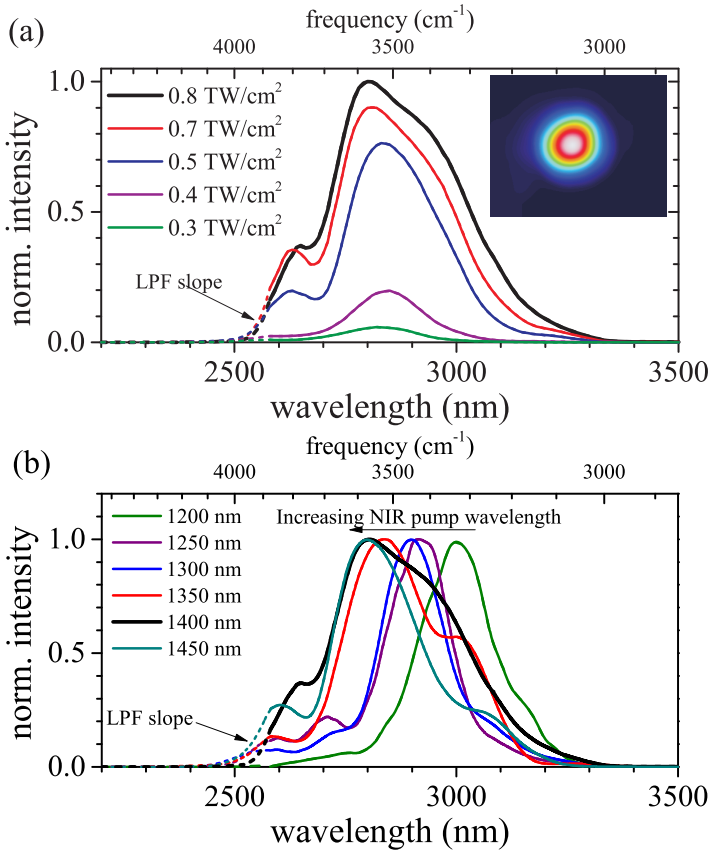

Fig. 2. Filtered MIR spectra (linear scale) using an LPF (cut-on wavelength 2.4 μm). (a) Evolution of the MIR spectrum for $\lambda_1 = 1.4$ μm and sweeping the pump intensity, but without changing the neutral density filter; the spectra are normalized to the peak intensity of the 0.8 TW/cm^2 case. Inset: beam profile of the filtered MIR pulse at 0.8 TW/cm^2. (b) Normalized spectra recorded under various NIR pump wavelengths and using the maximum intensity available (see Table 1).

show below the MIR part of the supercontinuum spectrum is caused by the NIR soliton emitting a phase-matched DW in the anomalous GVD regime of LN, which turns out to be in the MIR ($\lambda > \lambda_{ZD} = 1.92$ μm). The total bandwidth is around 1.5 octaves at -20 dB (spanning 163 THz, ranging from 3,175-8,600 cm^{-1}). This exceeds the 1.1 octave that we previously measured with this setup [26] (however, note that in [26] the MIR part of the spectrum was not measured).

The MIR DWs appear as prominent peaks beyond the dip around 2.5 μm. We applied an LPF with the cut-on wavelength of 2.40 μm (Edmund Optics) to filter away the soliton and harvest the MIR DW. Figure 2(a) shows a typical evolution under various pump intensities; note that the LPF slope affects the spectrum up to 2.58 μm, shown with dashed lines. The MIR DW first appears at the pump intensity of 0.3 TW/cm^2, and gradually builds up when the pump intensity further increases. At the maximum pump intensity the MIR bandwidth at -20 dB is 965 cm^{-1}, and covers the range from 3,000 cm^{-1} to 3,965 cm^{-1}.

The spatial quality of the filtered MIR pulses was also measured using an uncooled microbolometer camera (NEC, IRV-T0831). The inset of Fig. 2(a) shows a typical case, using

#223288 - $15.00 USD Received 14 Jan 2015; revised 3 Mar 2015; accepted 3 Mar 2015; published 6 Mar 2015

Table 1. Properties of the MIR DWs from in Fig. 2(b), including input wavelength λ_1, input energy W_1 and peak input intensity I_1. The DW center wavelength λ_{DW} is calculated as a weighted average over the filtered MIR spectrum. The MIR conversion efficiency η_{MIR} was found by measuring the power of the filtered and unfiltered case. The MIR bandwidth $\Delta\nu$ is shown as FWHM and at -20 dB.

λ_1	W_1	I_1	λ_{DW}	η_{MIR}	$\Delta\nu_{FWHM}$	$\Delta\nu_{-20dB}$
μm	μJ	TW/cm^2	μm	%	cm^{-1}	cm^{-1}
1.20	105	0.5	3.00	1.5	220	815
1.25	190	0.9	2.88	3.5	200	985
1.30	210	1.0	2.90	4.8	190	1,050
1.35	195	0.9	2.88	5.8	375	1,060
1.40	168	0.8	2.87	6.3	390	965
1.45	125	0.6	2.83	6.0	275	990

$\lambda_1 = 1.4$ μm and 0.8 TW/cm^2 case, evidencing that the generated MIR beam has a nice Gaussian beam profile. It here is worth to mention that even under the maximum pump intensities, the output beam is stable and accompanied with relatively pure visible color from SHG. This confirms that the total nonlinearity is self-defocusing, enabling a filament-free supercontinuum.

3.2. MIR wavelength tunability

Figure 2(b) shows the filtered DWs under various pump wavelengths from $1.20-1.45$ μm with 50 nm steps under the maximum input intensity available (see Table 1). All these wavelengths lie in the normal dispersion regime for the LN crystal. This means that this range supports a self-defocusing soliton. A MIR peak centered at 3.00 μm was obtained with the 1.20 μm pump and a MIR peak centered at 2.83 μm was found from 1.45 μm pump. This shows a tunability over nearly 200 nm.

This is the expected trend: when the pump wavelength decreases, the phase-matching wavelength of the MIR pulses increases. To see this, we need to look at the principle behind the DW formation, which is the well-known resonant phase-matching condition between a soliton and a linear (i.e. dispersive) wave. Specifically the DW phase-matching condition is $k_{sol}(\omega) = k_{DW}(\omega)$, where $k_{sol}(\omega) = k_e(\omega_{sol}) + (\omega - \omega_{sol})/v_{g,sol} + q_{sol}$ is the soliton wavenumber and $k_{DW}(\omega) = k_e(\omega)$ is the DW wavenumber, which simply follows the material dispersion, in this case $k_e(\omega) = n_e(\omega)\omega/c$. Here $n_e(\omega)$ is the linear refractive index of the *e*-polarized pump. The dispersion-free nature of the soliton is reflected in its linear dependence in frequency, i.e. it is a wave-packet traveling with the group velocity $v_{g,sol}$. There is also a nonlinear phase contribution to the soliton phase [37], which for cascaded SHG is $q_{sol} = n^I_{2,eff} I_{sol}\omega_{sol}/(2c)$ [23] where $n^I_{2,eff} = n^I_{2,casc} + n^I_{2,Kerr,el}$ is the effective nonlinear index, $n^I_{2,casc} = -2\omega_1 d^2_{eff}/[\varepsilon_0 c^2 n^2_e(\omega_1) n_e(\omega_2)\Delta k]$ the cascading nonlinear index and $n^I_{2,Kerr,el} = 3\chi^{(3)}/[4\varepsilon_0 c n^2_e(\omega_1)]$ is the Kerr electronic nonlinear index. For an effective defocusing nonlinearity ($n^I_{2,eff} < 0$) this nonlinear contribution will shift the phase-matching condition slightly towards longer wavelengths. However, for most cases this shift is insignificant compared to the impact of shifting the NIR soliton wavelength; thus, the tunability of the MIR DW relies mainly on tuning the NIR soliton wavelength, and the phase-matching curve for LN with $q_{sol} = 0$ can be found in Fig. 1(a) in [24].

The wavelength tunability of the MIR DWs with pump wavelength was weaker than expected from theory. According to Fig. 1(a) in [24] a pump soliton in the $1.20-1.45$ μm range should namely emit DWs with center wavelengths $\lambda_{DW} \sim 3.0-5.0$ μm, but instead we find $\lambda_{DW} \sim 2.8-3.0$ μm. Part of the explanation is to be found in the Raman-induced soliton self-frequency

#223288 - $15.00 USD Received 14 Jan 2015; revised 3 Mar 2015; accepted 3 Mar 2015; published 6 Mar 2015

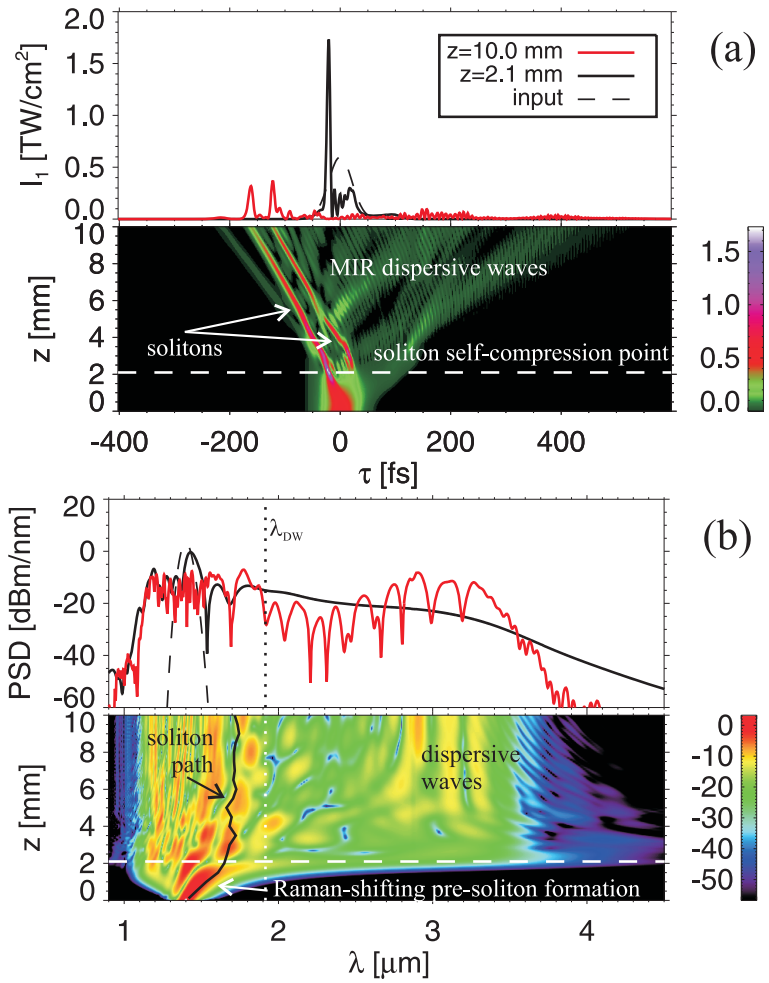

Fig. 3. Numerical simulation of pulse propagation in 10 mm LN. (a) Pump temporal intensity, (b) Pump power-spectral density (PSD). After 2.6 mm soliton self-compression occurs and two main solitons appear, which radiate MIR dispersive waves. The black curve "tracks" the soliton path. Input: 50 fs $\lambda_1 = 1.4$ μm and 0.6 TW/cm^2. A total Kerr nonlinear refractive index $n^I_{2,\mathrm{Kerr,tot}} = 54 \cdot 10^{-20}$ m^2/W and a Raman fraction $f_R = 0.35$ was used. The numerical model used plane-wave coupled envelope equations under the slowly-evolving wave approximation [30, 38]. The weak SH (containing less than 3% of the total energy) is not shown.

shift: LN has been found to have a significant Raman nonlinearity (see review in [39]), and the NIR soliton therefore will be significantly red-shifted compared to the input wavelength. This explains why DW radiation is found at shorter wavelengths than expected a priori from the input wavelength. However, the Raman soliton self-frequency shift alone cannot explain the results from Fig. 2.

3.3. Role of Raman effect in determining the MIR peak wavelengths

In order to understand this, we performed an extensive numerical study where we treated the total Kerr nonlinearity $n^I_{2,\mathrm{Kerr,tot}} = n^I_{2,\mathrm{Kerr,el}} + n^I_{2,\mathrm{Kerr,R}}$ and the Raman fraction $f_R =$

#223288 - $15.00 USD Received 14 Jan 2015; revised 3 Mar 2015; accepted 3 Mar 2015; published 6 Mar 2015

$n^I_{2,\mathrm{Kerr,R}}/n^I_{2,\mathrm{Kerr,tot}}$ as free parameters, but only varied within realistic limits of experimental measurements of $n^I_{2,\mathrm{Kerr,tot}}$ and the Raman gain (see more in [39]). It was possible to locate quite broad parameter ranges where the dispersive wave emission was more or less fixed around the $2.8-3.0$ μm regime. Figure 3 shows a characteristic example that showcases the typical dynamics well; $f_R = 0.35$ and $n^I_{2,\mathrm{Kerr,tot}} = 54\cdot 10^{-20}$ m^2/W was used. The large Raman fraction means that the Raman self-frequency shift will happen even before the soliton forms; as discussed in [40] the soliton spectral phase is affected by competing cascading and Raman effects, and when the Raman term is strong the spectrum will red-shift. We have illustrated this by indicating the soliton path, which was found by tracking the most intense part of the (τ,λ) spectrogram. Thus the first appearance of the dispersive wave at the soliton formation point will be phase-matched to a soliton with a wavelength significantly longer than the pump. This explains why in Fig. 3 the dispersive wave initially (at the soliton self-compression point, black line in the cuts) is centered around $3.3-3.5$ μm. This is significantly shorter than what one would expect with a soliton located at 1.4 μm, but it is consistent with the center wavelength of the main soliton. As the solitons are further Raman red-shifted the transfer of energy into dispersive waves becomes blue-shifted to below 3.0 μm. The solitons eventually experience the typical spectral recoil [8] as they approach the ZDW, and consequently the blue-shifting of the MIR dispersive waves is arrested. This is important because this seems to explain why despite the wide range of pump wavelengths and intensities that was used, we observed dispersive waves that were always centered around $2.8-3.0$ μm. Instead a "traditional" scenario would predict Raman red-shifting only after soliton formation, so the initial dispersive wave peak position lies at longer wavelengths and only then is it blue-shifted as the soliton is gradually red-shifted.

Some characteristics of these numerical results are backed up by the experiment. First Fig. 4 show how the spectral broadening develops when increasing the intensity. Figure 4(a) shows the low-intensity NIR development, and significant broadening starts to occur between 50 and 90 GW/cm^2, after which the new spectral shoulder clearly redshifts with increased intensity. This indicates that the Raman effect is indeed affecting the dynamics before soliton formation (no MIR DW radiation, the tell-tale sign of a soliton, was observed for these cases). Figure 4(b) shows the high-intensity development across the entire NIR and MIR; with these high intensities the MIR part of the spectrum started to appear. We note there are two DW peaks, since besides the main one just below 2.9 μm there is also a minor peak between $3.5-4.0$ μm. The presence of this minor peak leads us to believe that it is an early-stage DW emitted at the self-compression point when the soliton first forms. The low-wavelength major peak would then be a DW emitted at a later stage. The reason why the low-wavelength DW is dominating in the spectrum can then be explained by the Raman red-shifting effect: at the initial self-compression point the soliton has only been red-shifted slightly, and has therefore a phase-matched DW far into the MIR. This DW will therefore have a weak coupling to the soliton and thereby a low radiation efficiency. As the soliton propagates further it relaxes and recompresses, where it again will emit a dispersive wave. During this stage the Raman effect will red-shift the soliton further, which leads to a phase-matching condition at a shorter MIR wavelength, and hence the coupling to the soliton is much stronger leading to a higher MIR DW radiation efficiency. As the soliton comes closer to the zero-dispersion wavelength it will be spectrally recoiled so its redshifting will be arrested, and therefore the blue-shifting of the DW emission will also arrest.

Going back to the low-intensity dynamics of Fig. 4(a), we note that the spectrum is substantially broadened and red-shifted but the MIR DW radiation was not observed for these cases. For sure the lowest intensities are not enough to form a soliton, but as the intensity is increased the soliton onset will occur at some point. It is here relevant to point out that once the soliton formation threshold is crossed, it is still required to see a significant spectral broadening in or-

#223288 - $15.00 USD Received 14 Jan 2015; revised 3 Mar 2015; accepted 3 Mar 2015; published 6 Mar 2015

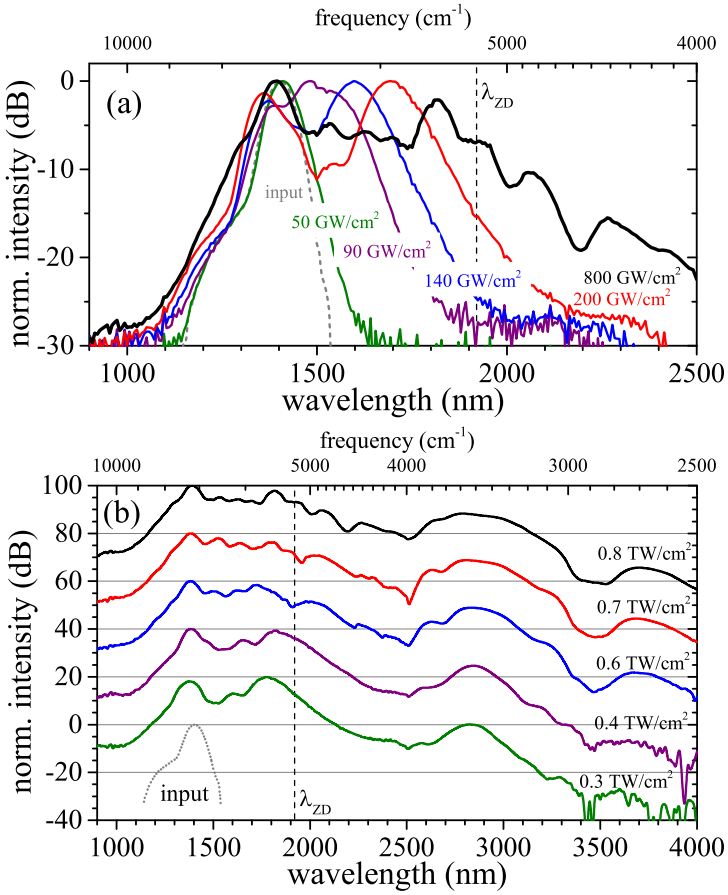

Fig. 4. Variation of the supercontinuum content at $\lambda_1 = 1.4\ \mu$m while sweeping the input peak intensity. (a) The NIR development at low intensities (where no MIR spectral content was measurable); for comparison the spectrum for the maximum intensity is also shown. (b) The full spectra at high intensities (a 20 dB offset per curve is used for clarity).

der to observe a MIR DW, i.e. a higher-order soliton must be excited. Once this happens the initial soliton self-compression point must occur within the relatively short crystal length we have chosen. Considering this, 200 GW/cm^2 might be enough for soliton self-compression to occur within 10 mm, and thereby also to form a DW. However, even if a soliton has formed already at this level, the coupling between the soliton and the DW is evidently not high enough for observing the MIR radiation. This would be in line the simulations of Fig. 3: at the soliton self-compression point the DW radiation is very weak, merely a bump on the soliton spectral tail. At 300 GW/cm^2 we do observe significant MIR radiation in form of DWs, and notice that the spectral shoulders of the soliton in the normal dispersion regime are located quite close to the zero-dispersion wavelength. This happens due to the Raman self-frequency shift. Usually a further increase in the intensity would lead to a stronger Raman red shift of the soliton spectrum, but the spectral recoil of the anomalous dispersion regime leads to a saturation of the red-shift: clearly the higher-intensity spectra do not present any change in the red-shift. This in turn leads to DWs that are emitted at roughly the same MIR wavelength, independent of the intensity. Therefore we conclude that the reason why the center wavelength of the major DW

#223288 - $15.00 USD Received 14 Jan 2015; revised 3 Mar 2015; accepted 3 Mar 2015; published 6 Mar 2015

remains fixed while sweeping the intensity, as in Fig. 2(a), is because the Raman self-frequency shift leads to a significant red-shift of the spectrum, so that at the onset of soliton-formation in the 10 mm crystal the red-shift is already close to saturation caused by the spectral recoil of the anomalous dispersion regime.

As a consequence of the dynamics suggested by this explanation, we should also see that the MIR DW changes its peak position upon propagation. We performed experiments in shorter crystals (3 and 5 mm), and saw that the MIR spectra after the LPF initially (3 mm) is located beyond 3.0 μm and that only later (5 and 10 mm) the sub-3.0 μm spectrum appears.

The Raman self-frequency shift can also explain the main DW has a relatively limited tuning range from $2.8-3.0$ μm. For low λ_1 the early-stage DW will be extremely weak because the phase-matching wavelength lies quite far away from the soliton. However, since the Raman effect will then shift the soliton we are able to observe a strong DW nonetheless, formed later in the crystal, but it is much more blue-shifted than what one would expect from the input wavelength as the soliton is now significantly red-shifted. Moreover, because the soliton red-shift will saturate, the low-wavelength input cases will not be so different from the high-wavelength input cases. That being said, we emphasize that there is a degree of tunability in the MIR pulses through the input wavelength, as Fig. 2(b) demonstrates, and we expect that by increasing the input wavelength further will extend the DW tunability to wavelengths shorter than 2.8 μm. It is also worth to note that LN is well-known to have a relatively strong Raman nonlinearity, so we expect that with other crystals with a less dominating Raman nonlinearity will show stronger tunability concerning the DW wavelength.

3.4. MIR conversion efficiency and energy scaling capabilities

The average power of the filtered MIR pulse was measured to 10.5 mW with 168 mW pump power at 1.40 μm, corresponding to an overall NIR to MIR energy conversion efficiency of $\eta_{\mathrm{MIR}} = 6.3\%$. We generally find $\eta_{\mathrm{MIR}} = 4-6\%$ (see Table 1), except for $\lambda_1 = 1.20$ μm, where it is $\eta_{\mathrm{MIR}} = 1.5\%$. We expected this case to have the lowest efficiency because it had λ_1 furthest away from λ_{ZD} and thereby also the phase-matching point further into the MIR than the other cases; this naturally gives a lower coupling efficiency. Moreover, the lower OPA output gave a significantly lower peak input intensity than the other cases, and as the GVD increases at shorter wavelengths this all leads to a lower soliton order and thus a reduced spectral broadening. These factors combined are behind the lower MIR conversion efficiency at 1.20 μm.

Because we exploit a noncritical cascaded SHG interaction, the soliton formation and MIR DW generation is rather insensitive to the crystal angle adjustment, which is quite different from the critical phase-matching condition required by other techniques like OPA. Moreover, the conversion efficiency is already comparable with the traditional DFG process under critical phase-matching conditions and synchronized pump wavelengths. We could actually expect much higher conversion efficiencies when pumping closer to the zero-dispersion wavelength (see [24]), with the tradeoff that the DW will be generated closer to the pump wavelength as well. This is because the DW energy is proportional to the soliton spectral overlap at the radiated frequency, so the closer we pump to the zero-dispersion wavelength, the more energy will reside in the DW.

We used few-GW peak-power pump pulses as this was the limit of our OPA, but our scheme also supports higher peak powers because it is filament-free due to the self-defocusing nonlinearity. This gives a strong scalability with input energy. Consider, e.g., using a TW-peak power Cr:forsterite laser amplifier (sub-100 fs $>$100 mJ pulses at 1250 nm), and with 3% efficiency this could generate around 3 mJ MIR energy in a 10 mm long LN crystal provided that the crystal aperture is increased to around 40×40 mm^2. Such a large aperture is only possible because periodic poling is not needed. The MIR spectral density would be close to 1 mW/nm at a 10 Hz

#223288 - $15.00 USD Received 14 Jan 2015; revised 3 Mar 2015; accepted 3 Mar 2015; published 6 Mar 2015

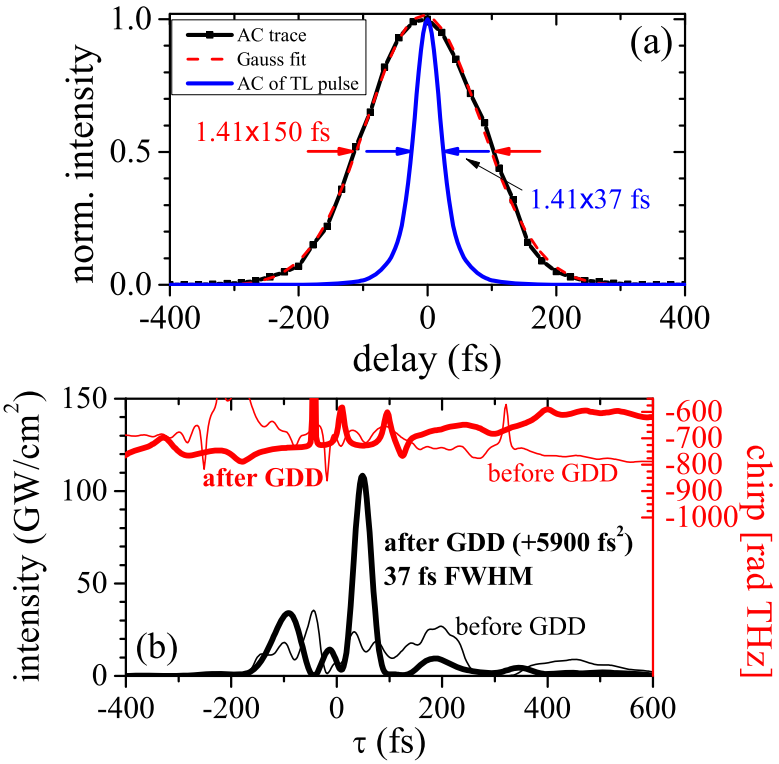

Fig. 5. (a) Typical intensity autocorrelation trace for the filtered MIR pulses generated by a 1.3 μm pump with $I_1 = 1.0$ TW/cm^2. The blue curve shows the transform-limited pulse duration of the filtered MIR spectrum. (b) Numerical example of a MIR DW when the near-IR part is removed (using the same LPF as in the experiment); the case from Fig. 3 is shown. The MIR pulse is quite broad and complex, but by simply applying a suitably selected amount of positive GDD the MIR pulse is compressed to sub-40 fs FWHM.

repetition rate.

3.5. Temporal characterisation of the MIR pulses

We temporally characterized the MIR DWs with a home-made MIR SHG intensity autocorrelator, consisting of a ZnSe beam splitter and a 0.4-mm-thick $AgGaS_2$ crystal ($\theta = 39°$, $\phi = 45°$, Eksma Optics). A typical measurement for $\lambda_1 = 1.30$ μm is shown in Fig. 5(a). The pulse duration is 150 fs assuming a Gaussian shape. Similarly, for $\lambda_1 = 1.40$ μm we obtained a 190 fs pulse duration, and between 145 to 210 fs at the other pump wavelengths. In Fig. 5(a) the autocorrelation trace for a transform-limited pulse calculated from the filtered MIR spectrum is also shown, and it gives $\simeq 40$ fs at 3.0 μm wavelength, corresponding to 4 optical cycles. The generated MIR pulses are therefore quite chirped. This is expected as the soliton self-compression point occurs quite early inside the crystal, and after this the DW accumulates phase according to the material dispersion (see also [24]). The accumulated chirp will be quite linear as GVD is the dominating dispersion at the MIR wavelength. Thus, significant pulse compression should be possible by compensating the linear chirp with a dispersive element.

The simulations presented in Fig. 5(b) support this idea: the result from Fig. 3 was spectrally filtered as in the experiment so the MIR spectral components beyond 2.4 μm remained. The temporal profile reveals a broad pulse with an $>$ 600 fs envelope. We then compensated

#223288 - $15.00 USD Received 14 Jan 2015; revised 3 Mar 2015; accepted 3 Mar 2015; published 6 Mar 2015

the quadratic spectral phase components of this pulse by applying a suitable amount of positive group-delay dispersion (GDD); practically this can be done with a short piece of MIR transparent glass. This resulted in a short sub-40 fs and intense MIR pulse.

4. Conclusion

Concluding, we experimentally observed high-energy efficient and broadband femtosecond MIR wave generation using a NIR femtosecond pump and a short bulk quadratic nonlinear crystal. These MIR waves were generated by exciting self-defocusing NIR solitons, induced by a cascaded quadratic $\chi^{(2)}$ nonlinearity, and these solitons emitted DWs in the anomalous GVD regime in the MIR. Broadband, femtosecond MIR pulses tunable from $2.8-3.0$ μm were obtained through a 10-mm-long bulk lithium niobate crystal and the tunability can be expanded by pumping over a broader wavelength range. The largest MIR bandwidth generated was almost 1,100 cm^{-1}, and covered the range from $3,000-4,100$ cm^{-1}. The pulse durations for the generated MIR pulses were measured to be $\sim 145-210$ fs FWHM. This indicates an additional spectral phase that we expect mainly comes from dispersive propagation in the crystal, so obtaining much shorter few-cycle pulses should be possible after simple dispersion compensation. Weaker MIR DW emission was found up to 4.0 μm (2,500 cm^{-1}). Combining the experimental data with numerical simulations we found that the soliton dynamics and thereby also DW formation seem strongly influenced by Raman self-frequency shifting of the input pulse *prior* to soliton formation as well as the usual Raman soliton self-frequency shifter *after* soliton formation. The most energetic MIR pulse contained 10.5 μJ of energy, corresponding to 6.3% NIR-to-MIR conversion efficiency. This is comparable to the commonly used OPA/DFG techniques for high-energy MIR pulse generation, and also in other features does the demonstrated method compete well as it shows great simplicity: it does not require synchronized pump wavelengths or critical phase-matching conditions, and it should scale linearly with an increased pump pulse energy. Although our experiment relied on an OPA stage to provide a pump pulse with an NIR input wavelength suitable for the chosen LN crystal, it is possible to pump the crystal directly with the output of a laser amplifier; for the LN crystal a Cr:forsterite based laser system is particularly suitable.

The simplicity of the setup is further emphasized by the fact that no periodic poling of the quadratic nonlinear crystal is required, implying that large-aperture low-cost and low-complexity crystals can be used. This paves way for a wide range of NIR and MIR nonlinear crystals with large diagonal tensor nonlinearities, which could be used to realize coverage in various MIR wavelength regimes. One specific example is the biaxial $LiInS_2$ crystal cut for noncritical interaction, which when pumped in the short wavelength range of the MIR should give a DW in well into the MIR [41, 42]. This would target a different MIR regime where carbon double and triple bonds have characteristic resonance frequencies and where ultrafast spectroscopy of water is performed to study the H-O-H bending dynamics. We hope this work could pave the way for a new kind of ultrafast MIR source, which could be a important complement for the OPA/DFG MIR sources.

Acknowledgments

The Danish Council for Independent Research (11-106702).

#223288 - $15.00 USD Received 14 Jan 2015; revised 3 Mar 2015; accepted 3 Mar 2015; published 6 Mar 2015